

## Applicability of Equivalent Linear Three-Dimensional FEM Analysis of Reactor Buildings to the Seismic Response of a Soil–Structure Interaction System

Yoshitaka Ichihara<sup>1,2</sup>, Naohiro Nakamura<sup>3</sup>, Kunihiko Nabeshima<sup>4</sup>, Byunghyun Choi<sup>5</sup>, Akemi Nishida<sup>6</sup>

<sup>1</sup> Doctoral Course, Graduate School of Advanced Sci. and Eng., Hiroshima Univ., Japan

<sup>2</sup> Chief, Power Eng. Dept., Takenaka Corp., M. Env., Japan (ichihara.yoshitaka@takenaka.co.jp)

<sup>3</sup> Prof., Graduate School of Advanced Sci. and Eng., Hiroshima Univ., Dr. Eng., Japan

<sup>4</sup> Assistant Prof., Graduate School of Advanced Sci. and Eng., Hiroshima Univ., Dr. Eng., Japan

<sup>5</sup> Assistant Principal Researcher, NSRC, Japan Atomic Energy Agency, Dr. Eng., Japan

<sup>6</sup> Senior Principal Researcher, NSRC, Japan Atomic Energy Agency, Dr. Eng., Japan

### ABSTRACT

This paper evaluates the applicability of equivalent linear analysis of reinforced concrete, which uses frequency-independent complex damping with a small computational load, to the seismic design of nuclear power plant reactor buildings. To this end, a three-dimensional finite element method analysis of the soil–structure interaction focusing on nonlinear and equivalent linear seismic behavior of the building embedded in an ideally uniform soil condition (shear wave velocity  $V_s = 880$  m/s) was performed for the Kashiwazaki–Kariwa Nuclear Power Plant Unit 7 reactor building. The equivalent linear analysis results correlated well with the nonlinear analysis results of the shear strain, acceleration, displacement, and acceleration response spectrum, demonstrating the effectiveness of the equivalent linear analysis method. Moreover, the equivalent linear analysis results were more conservative than those of nonlinear analysis using the material constitutive law in evaluating the shear strain of the external wall of the reactor building. From this observation, equivalent linear analysis tended to obtain a lower building stiffness than nonlinear analysis under the analysis conditions used in this paper. The equivalent linear analysis calculation results should be conservative in shear strain evaluation for seismic safety.

### INTRODUCTION

Overall, seismic response analysis of heavy, large, and rigid reinforced concrete (RC) structures cannot ignore the effect of soil–structure interaction (SSI). Therefore, buildings, such as the reactor building (RB) of a nuclear power plant (NPP), are seismically designed using a soil–structure coupled system that considers the effect of the soil. Ichihara et al. conducted a seismic response analysis of the RB of an advanced boiling water reactor (ABWR) considering SSI using a three-dimensional (3D) finite element method (FEM) model with detailed modeling of the surrounding soil (Ichihara et al., 2021a; 2021b). However, this analysis was mainly based on the assumption that the behavior of the building was linear, referring to the results of previous studies. Although the nonlinear behavior of RC structures was considered in part of the analysis, the effects of noise due to the convergence conditions of the nonlinear analysis were observed, and the stability and accuracy of the obtained results remained problematic. Therefore, it is necessary to address the remaining problems to accurately evaluate the 3D response characteristics of buildings for various seismic input levels. Accurately analyzing SSI of the nonlinear behavior of buildings, as performed by Nakamura et al. (2010), is crucial to clarify the behavior of RBs and improve the seismic safety of NPP facilities. However, nonlinear 3D FEM analysis based on the conventional material constitutive law requires detailed FEM modeling, including the surrounding soil, which requires several weeks for a single analysis even with current high-performance computers. Accordingly, it is vital to

determine how to reduce the computational load suitable for practical use.

Ghiocel proposed a method to consider the effect of nonlinearity of RC materials in 3D FEM analysis in the frequency domain using the restoring force characteristics of RC seismic walls, similar to the equivalent linear analysis of soil performed by the SHAKE computer program (Schnabel et al., 1972). In the equivalent linear analysis of soil for NPP facilities in Japan, a lower limit of 0.7 has been established as the average stiffness reduction ratio of the supporting soil (Japan Electric Association [JEA], 2017), and its application to the equivalent linear analysis of RBs can also be expected within a certain range. Furthermore, taking the equivalent linear analysis of soil as an example, the analytical conditions are simpler than those of nonlinear analysis, and the computation time is shorter. Furthermore, stable results can be obtained, and frequency-independent complex damping can be achieved. Therefore, equivalent linear analysis is suitable for practical SSI analysis. However, studies on the equivalent linear analysis of RC primarily compared the nonlinear analysis results with the equivalent linear analysis results of simple RC structures and did not verify using equivalent linear analysis for actual NPP facilities. Therefore, this paper evaluates the applicability of the equivalent linear analysis method for RC proposed by Ghiocel (2015) to NPP facilities by performing 3D FEM SSI analysis under ideal soil conditions. The target building is the Kashiwazaki–Kariwa NPP Unit 7 RB of ABWR, used in the Kashiwazaki–Kariwa Research Initiative for Seismic Margin Assessment benchmark analysis conducted by the International Atomic Energy Agency (IAEA; IAEA, 2013). The accuracy of the analysis method is evaluated by comparing it with that of nonlinear 3D FEM analysis using the RC constitutive law, which focuses only on the nonlinear characteristics of the structure. This paper is based on Ichihara et al. (2022b), published in Japanese.

## PREVIOUS STUDY ON APPLICABILITY OF EQUIVALENT LINEAR 3D FEM

In a study on the equivalent linear analysis of RC, Ichihara et al. (2022a) demonstrated that the response compares to the response of nonlinear analysis up to RUN 4 (shear wall strain of approximately  $\gamma = 2.0 \times 10^{-3}$ ) from simulation analysis through verification with the Seismic Ultimate Dynamic Response Test of the RB provided by the Nuclear Power Engineering Corporation of Japan for the Seismic Shear Wall International Standard Problem (OECD/NEA/CSNI, 1996) in 1996. Figures 1–3 present examples of the analysis by Ichihara et al. (2022a), namely, comparisons of the analysis and test results of the acceleration response, the inertia force–displacement relationship, and the acceleration response spectrum of the top slab. In these figures, the NL and EQ models represent the nonlinear analysis and equivalent linear models, respectively. The vibration levels covered by these figures are RUN 1 (small-amplitude level in the elastic region), RUN 4 (approximately  $\gamma = 2.0 \times 10^{-3}$ ), and RUN 5 (ultimate shear wall strain of approximately  $\gamma = 4.0 \times 10^{-3}$ ). From these analysis results, Ichihara et al. (2022a) concluded that the accuracy of the EQ model is comparable to that of the NL model for responses up to RUN 4. However, whether the EQ model's results can be directly applied to buildings with complex structures, such as RBs, was not investigated. Therefore, to extend the scope of application of equivalent linear analysis to the practical level in the nuclear field, it is necessary to verify the method using full-scale buildings while considering the effect of SSI.

## ANALYSIS METHOD AND CONDITIONS

### *Nonlinear Analysis*

For nonlinear analysis, FINAS/STAR was used, as by Ichihara et al. (2022a), and the layered shell element (Fig. 4) represents the RC material's nonlinearity. The nonlinear characteristics of tension (Fig. 5[a]), compression (Fig. 5[b]), cracks (smeared crack model), and shear stiffness of the cracked elements of the concrete wall were also modeled as by Ichihara et al. (2022a). Additionally, the nonlinear properties of concrete were the same as the stress–strain relationship proposed by the IAEA, where the bond-slip between the reinforcement and concrete was assumed to be ignored (fully bonded) and its effect was represented by parameter C ( $C = 0.4$ ). The reinforcement was uniaxial material with bilinear restoring force characteristics. The second gradient of the restoring force characteristics was 1/100 of the initial stiffness. The time

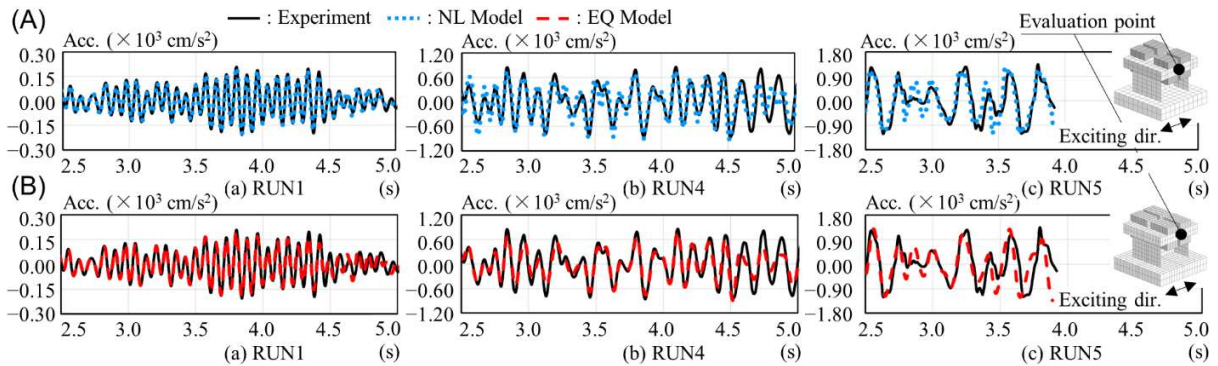


Fig. 1 Comparison of analysis and test results of acceleration (Acc.) for (A) NL and (B) EQ models (Ichihara et al., 2022a)

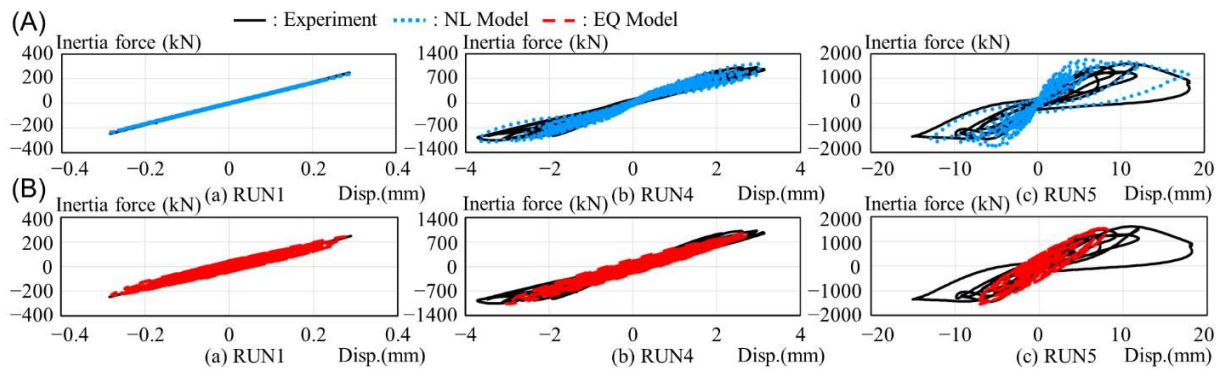


Fig. 2 Comparison of analysis and test results of the inertia force–displacement relationship for (A) NL and (B) EQ models (Ichihara et al., 2022a)

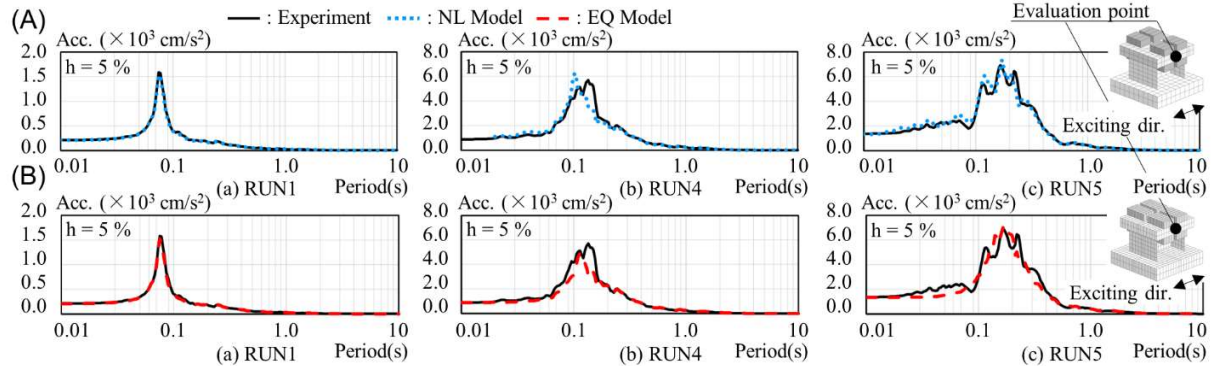


Fig. 3 Comparison of analysis and test results of acceleration (Acc.) spectra for (A) NL and (B) EQ models (Ichihara et al., 2022a)

integration method was the Newmark- $\beta$  method, and the coefficients  $\beta$  and  $\gamma$  were  $\beta = 1/4$  and  $\gamma = 1/2$ . If convergence was not achieved after three runs, the residual force was carried over to the next analysis step. The time step of the nonlinear analysis was 0.001 s.

### **Equivalent Linear Analysis**

For equivalent linear analysis, an ACS SASSI (GP Technologies, 2019) was used, as by Ichihara et al. (2022a). The calculation procedure of the equivalent linear analysis is presented in Fig. 6, where  $S_f$  is the

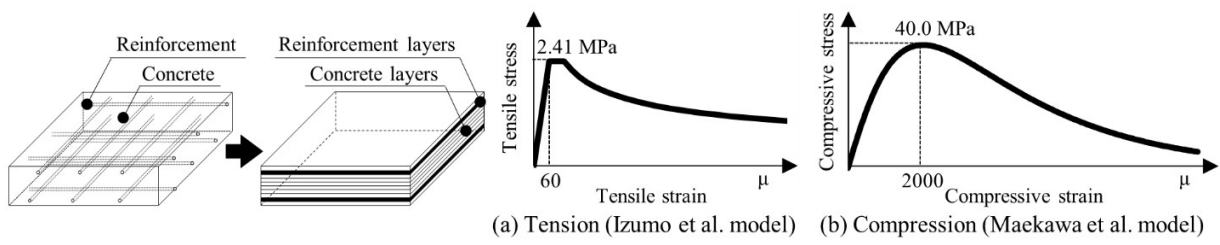


Fig. 4 Layered shell element for RC  
(Ichihara et al., 2021b)

Fig. 5 Modeling of nonlinear characteristics of RC shear walls  
(Ichihara et al., 2022b)

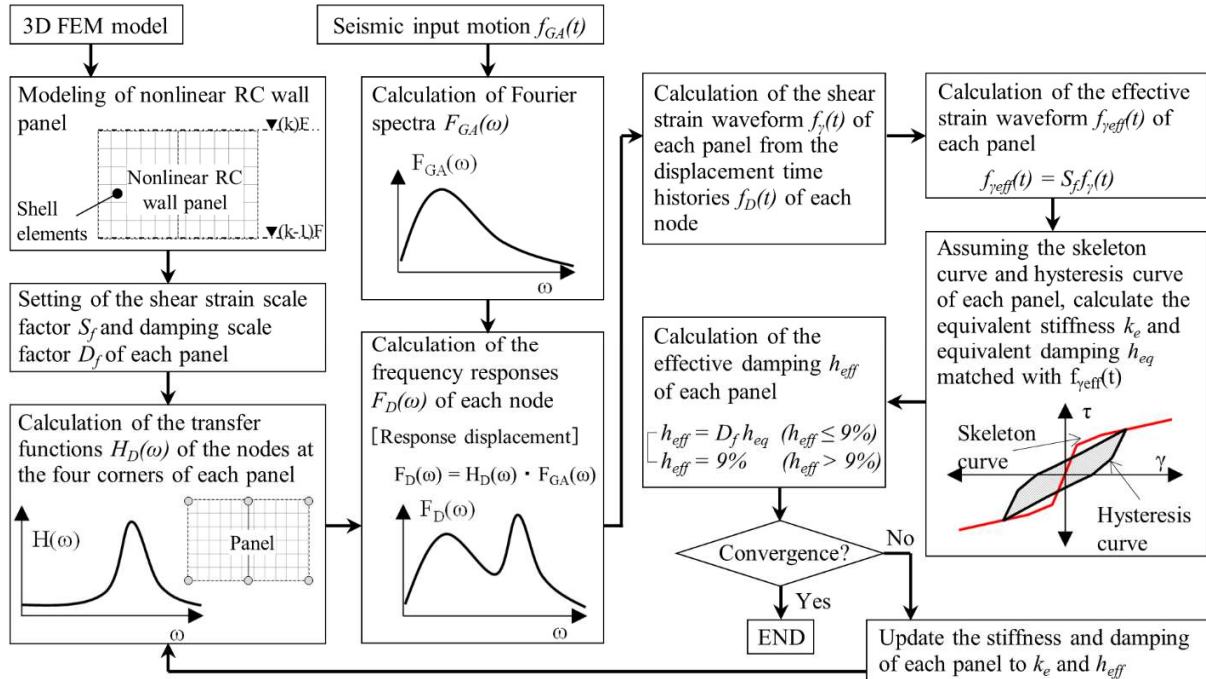


Fig. 6 Calculation procedure of equivalent linear analysis (Ichihara et al., 2022a)

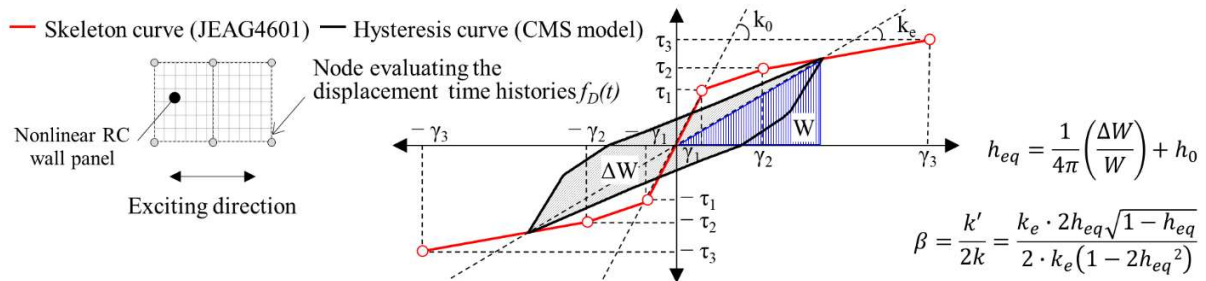


Fig. 7 Restoring force characteristics of RC shear wall (Ichihara et al., 2022a)

shear strain scale factor and  $D_f$  is the damping scale factor. Option NON, which is an analysis function of ACS SASSI, was used to evaluate the equivalent stiffness  $k_e$  and equivalent damping  $h_{eq}$  of the wall. Option NON evaluates  $k_e$  and  $h_{eq}$  for each panel from the in-plane shear strain in the nonlinear RC wall panel. The nonlinear RC wall panel is a group of linear shell elements in the wall and is a parameter set by the analyst presented in Fig. 6. In the equivalent linear analysis of soil represented by SHAKE (Schnabel et al., 1972), it is necessary to set a coefficient that multiplies the maximum value of the strain waveform when

determining the effective strain. Similarly, in the equivalent linear analysis of RC using Option NON, it is necessary to set  $S_f$  and  $D_f$  as parameters when obtaining stiffness and damping equivalent to the nonlinear response. These parameters were  $S_f = 0.7$  and  $D_f = 1.0$  for each nonlinear RC wall panel based on the results of Ichihara et al. (2022a). Note that the nonlinear RC wall panel was coarsely set to approximately one division between floor heights and one division between grid lines (excluding the area around openings), referring to the results of Ichihara et al. (2022a).

Figure 7 shows the restoring force characteristics of the RC seismic wall used in an equivalent linear analysis of RC, where  $k_0$  is the initial stiffness,  $h_0$  is the initial damping constant,  $\Delta W$  is the consumed energy per cycle of the hysteresis loop,  $W$  is the equivalent potential energy,  $\beta$  is the complex damping constant,  $k$  is the real part of the complex spring,  $k'$  is the imaginary part of the complex spring, and  $\tau_{1-3}$  and  $\gamma_{1-3}$  are the shear stress and shear strain at the first to third yielding points, respectively. The first, second, and third yielding points in the figure correspond to the approximate value at which shear cracks begin to appear near the center of the RC seismic wall, the approximate value at which the reinforcement starts to yield, and the approximate value at which ultimate failure occurs, respectively. In this study,  $k_e$  was obtained by the secant stiffness connecting the maximum displacement point in the hysteresis loop with the origin, and  $h_{eq}$  was obtained by adding  $h_0$  to the relationship between  $\Delta W$  and  $W$  per cycle of the hysteresis loop. Note that  $h_{eq}$  was considered the complex stiffness in the analysis. The skeleton curve of the RC seismic wall was determined from the Technical Code for Seismic Design of Nuclear Power Plants (JEA, 2017), which was established based on test data performed on an RB. The hysteresis curve was the Cheng–Mertz shear model (Cheng et al., 1989). The upper limit of the effective damping  $h_{eff}$  was set to  $h_{eff} = 9\%$  based on the results of Ichihara et al. (2022a). Since equivalent linear analysis using Option NON does not apply to a cylindrical wall in the center of a building,  $k_e$  and  $h_{eff}$  were instead estimated from the results of Ichihara et al. (2022a). The convergence of the iterative equivalent linear analysis was determined based on an equation where the stiffness reduction ratio  $k_e/k_0$  of the nonlinear RC wall panel was weighted and averaged by the volume  $V$  of the panel. The convergence condition was that the residual difference between iterations  $k$  and  $k-1$  was less than 1%, or the number of iterations reached 9.

## ANALYSIS MODEL

### *Structural Model*

Figure 8 presents the plan and cross-section of the building. For the building, only the ABWR type of Kashiwazaki–Kariwa NPP Unit 7 RB, which was the subject of IAEA (2013), was employed, and the effects of adjacent buildings, separation and sliding of soil from the sidewall, and foundation uplift were not considered. Note that T.M.S.L. in the figure denotes Tokyo Mean Sea Level. Table 1 presents the structural materials and physical properties of the building. The RC materials were either nonlinear or equivalent linear, whereas the steel materials were only linear. Table 2 displays the floor level (FL) and weight distribution of the building. The structure's weight was density-adjusted at the FL position so that the 3D FEM model's weight matched the IAEA (2013) lumped-mass stick model's (LMSM's) weight distribution. Figure 9 presents the structural model. For the structure, the walls of the NL and EQ models were layered shell elements (see Fig. 4) and shell elements, respectively. The remainder of the structure was modeled with the same elements: solid elements for the base slab, shell elements for the floor slab, beam elements for the columns and beams, and one-dimensional rod elements for the diagonal members, struts, and horizontal brace that constituted the roof slab. The mesh size was set so that the spaces between the grid lines on the plan and between floors in elevation were divided into four to five sections. Openings in the walls and floors were reflected in the structural model only for major openings. For large equipment inside the containment vessel, only weight was considered and was entered as a uniform load on the floor slab. Note that the NL and EQ models referred to here are the same 3D FEM models used for nonlinear and equivalent linear analyses by Ichihara et al. (2022a).

The damping of the structure in the NL model was set to be Rayleigh damping; thus, concrete damping  $h_c$  and steel damping  $h_s$  were set to  $h_c = 5\%$  and  $h_s = 2\%$  for the average fundamental frequency

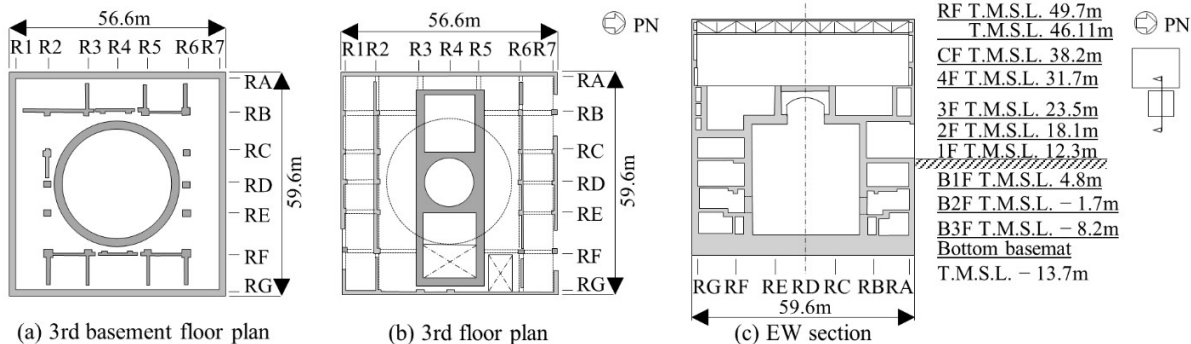


Fig. 8 Plans and cross-section of RB (Ichihara et al., 2021b)

Table 1 Structural materials and properties (Ichihara et al., 2022b)

Material	Structural parts	Measured concrete strength or steel reinforcement tensile strength	Structural parts or types	Young modulus E (MPa)	Shear modulus of elasticity G (MPa)	Poisson ratio v	Weight density $\gamma$ (kN/m <sup>3</sup> )
Concrete	Basemat	44.1	Basemat	29,000	12,100	0.20	23.5
	Structure	49.0		31,300	13,100	0.20	24.0
Steel		490	Steel Reinforcement	205,000	—	—	77.0
			Steel	205,000	79,000	0.30	77.0

Table 2 Floor level and weight distribution of LMSM and 3D FEM model (Ichihara et al., 2021b)

RB				RCCV			
Floor	Elevation T.M.S.L. (m)		Weight (kN)	Floor	Elevation T.M.S.L. (m)		Weight (kN)
	LMSM	3D FEM model			LMSM	3D FEM model	
RF	49.70	49.70	—	43.95	39,760		
CF	38.20	43.95	—	34.95	80,820		
4F	31.70	34.95	—	27.60	86,110		
3F	23.50	27.60	—	20.80	86,400		
2F	18.10	20.80	—	15.20	56,460		
1F	12.30	15.20	—	8.55	82,650		
B1F	4.80	8.55	—	1.55	81,700		
B2F	-1.70	1.55	—	-4.95	82,900		
B3F	-8.20	-4.95	—	-10.95	349,200		
Basemat	-13.70	-10.95	—	-13.70	220,300		
			Total		1,991,700		

in the north-south (NS) and east-west (EW) directions (4.49 Hz) and the fundamental frequency in the up-down (UD) direction (11.00 Hz) when the base was fixed. Structural damping in the EQ model was complex damping, with  $h_c = 5\%$  and  $h_s = 2\%$ .

### Soil Model

Based on Ichihara et al. (2021a), the soil was assumed to be ideally uniform and elastic without any heterogeneity, different from the actual soil. Table 3 presents the soil properties, and Fig. 10 shows the NL soil model. The soil of the NL model was modeled horizontally with FEM solid elements to approximately five times the width of the base. The mesh size was modeled up to T.M.S.L. -155 m, referring to the mesh size of the structure. The sides of the soil model were set as periodic boundaries, and the bottom was set as a viscous boundary. The soil of the EQ model was modeled by the thin layer element method. The vertical mesh size was the same as the NL model and was modeled up to T.M.S.L. -155 m. The damping of the soil in the NL model was Rayleigh damping, and the damping constants of the soil were consistent with those in Table 3 for the average fundamental frequencies in the NS and EW directions (1.32 Hz) when the

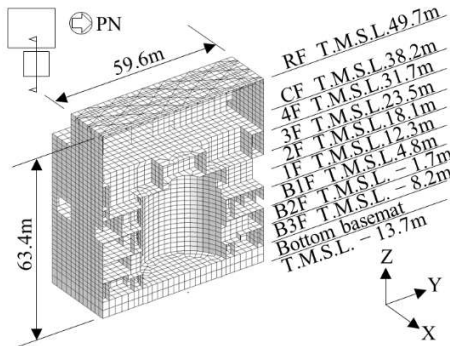


Table 3 Soil properties  
 (Ichihara et al., 2021a)

Shear wave vel. $(V_s)$ (m/s)	880
Primary wave vel. $(V_s)$ (m/s)	2320
Poisson ratio $(\nu)$	0.416
Unit weight $(\gamma)$ (kN/m <sup>3</sup> )	19.9
Damping constant $(h)$ (%)	3

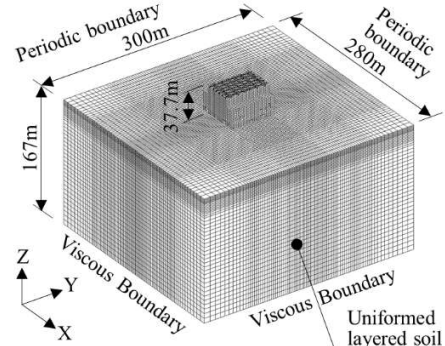


Fig. 9 Structural model (Ichihara et al., 2022b) Fig. 10 Soil model for NL model (Ichihara et al., 2022b)

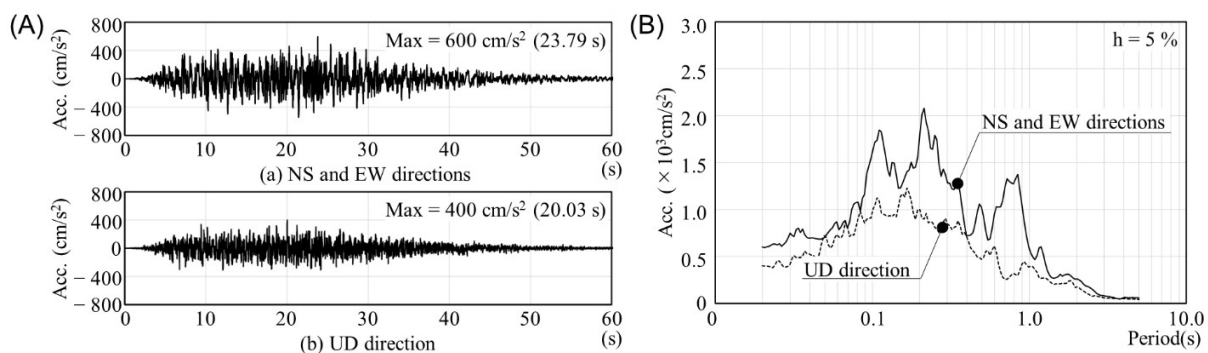


Fig. 11 Seismic input at GL for (A) acceleration (Acc.), (B) Acc. response spectra (Ichihara et al., 2022b)

Table 4 Comparison of fixed-base fundamental frequencies (Ichihara et al., 2022b)

	Frequency (Hz)		
	NS	EW	UD
NL model	4.19	4.79	11.00
Mean of IAEA (IAEA, 2013)	4.56	4.96	8.22

Table 5 Comparison of fundamental frequencies with SSI models (Ichihara et al., 2022b)

	Frequency (Hz)	
	NS	EW
NL model	1.32	1.32
EQ model	1.37	1.37

SSI was considered and the fundamental frequency in the UD direction (11.00 Hz) when the base was fixed. In contrast, soil damping in the EQ model was complex damping, and the damping constant listed in Table 3 was used. The integration (NL model) and dynamic substructure methods (EQ model) represent the interaction.

### Seismic Input

Seismic input was applied simultaneously in three directions, and the waveforms conforming to the response spectrum by JEA were prepared. Figure 11 displays the outcrop motion defined at the ground level (GL) (T.M.S.L. +12.0 m). The earthquake motions in the NS and EW directions were assumed to be the same phase input. The analysis was 20 s from approximately 9 to 29 s, corresponding to the main motion in the NL model and was the entire analysis time in the EQ model. The maximum acceleration response was 600 cm/s<sup>2</sup> horizontally and 400 cm/s<sup>2</sup> vertically at the GL.

## ANALYSIS RESULTS

### Eigenvalue and Dominant Frequency

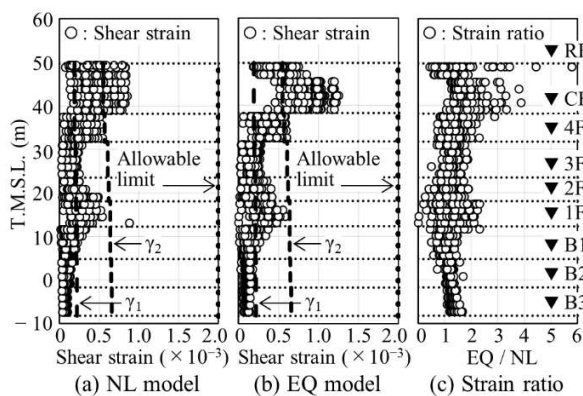


Fig. 12 Comparison of maximum shear strain and ratio distributions of external walls in NS direction (Ichihara et al., 2022b)

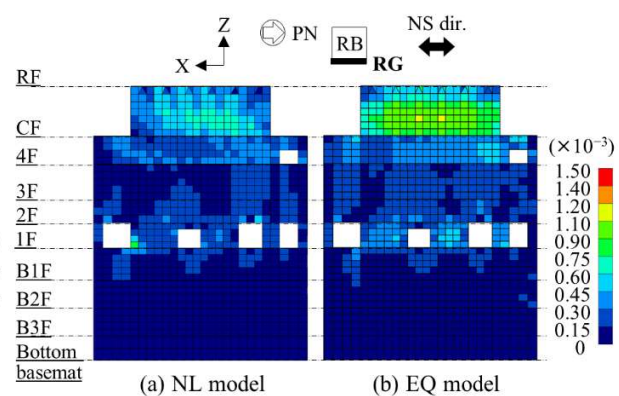


Fig. 13 Maximum shear strain contours for NL and EQ models of line RG external wall

To validate the structural model, the NL model was used as a baseline, its base position was fixed, and eigenvalue analysis was performed. Table 4 presents the fundamental frequencies of the NL model. Table 4 presents the mean fixed-base fundamental frequencies reported by IAEA (2013) for comparison. The table indicates that the NL model's fundamental frequencies were consistent with the IAEA results in NS and EW directions, although there were some discrepancies between the mean of the IAEA results (2013). For the UD direction, in contrast, there was a considerable difference between the results of the NL model and the mean of the IAEA results (2013) because the NL model captures the out-of-plane response of coupled floor slabs of the roof floor (RF) and crane floor (CF) as a first-order eigenmode, whereas the mean of the IAEA results (2013) captures the response of the RF slab alone as a primary mode. Next, to validate the interaction model, eigenvalue analysis of the NL model was performed and compared with the mean dominant frequencies at the four corners of the CF obtained from the EQ model. The dominant frequency was determined as the Fourier spectral ratio for the T.M.S.L. -155 m input motion. Table 5 compares each model's fundamental and dominant frequencies, indicating that the NL and EQ models correlated well with the NS and EW directions with negligible differences.

### **Comparison of Time History Response and Frequency Response**

Figure 12 presents the shear strain and shear strain ratio distributions of each model for the external walls of each floor of the building. Here, the shear strain ratio distribution was calculated as the ratio of the shear strain of the EQ model to the shear strain of the NL model. Figure 12 displays the maximum shear strain for each finite element in the NS and EW directions, where the building stiffness was small and the response was large. In the evaluation in Figs. 12(a) and 12(b), the shear strains ( $\gamma_1$  and  $\gamma_2$ ) at the first and second yielding points defined by the skeleton curve of the RC seismic wall and the allowable limit of the RC seismic wall to the design-basis ground motion  $S_s$  ( $\gamma = 2.0 \times 10^{-3}$ ) (JEA, 2017) were plotted as reference values. In Figs. 12(a) and 12(b), the shear strain distributions of both models indicate that the shear strains were large near the first floor (1F), fourth floor (4F), and CF. Observing individual finite elements, they were well below the allowable limits, although they exceeded  $\gamma_2$  in some areas. Next, by comparing the NL and EQ models, the individual elements in the EQ model began to exceed  $\gamma_1$  in floors above 1F, where the plasticity increased. The shear strain of the EQ model tended to be larger than the shear strain of the NL model. From Fig. 12(c), the shear strain ratio varied greatly in the range of plasticity, indicating that the RC constitutive law or equivalent stiffness accounted for the nonlinearity of RC materials. Furthermore, focusing on individual elements, the shear strain ratio was generally above 1.0, indicating that the shear strain of the EQ model was evaluated to be larger than the shear strain of the NL model. Figure 13 presents the maximum shear strain contours for the NL and EQ models. This figure indicates that the maximum shear strain of the EQ model was generally larger than that of the NL model, although it was locally lower

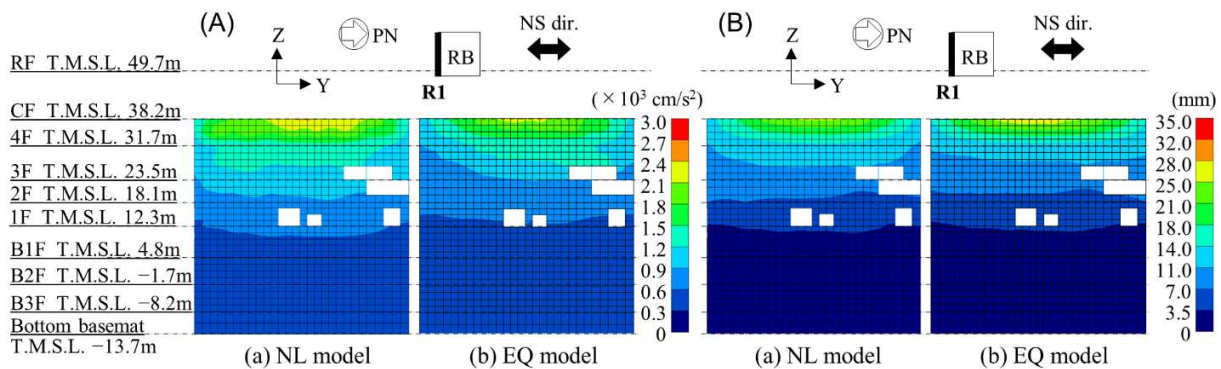


Fig. 14 Comparison of (A) acceleration response contour and (B) displacement response contour for the NL and EQ models of line R1 external walls (out-of-plane)

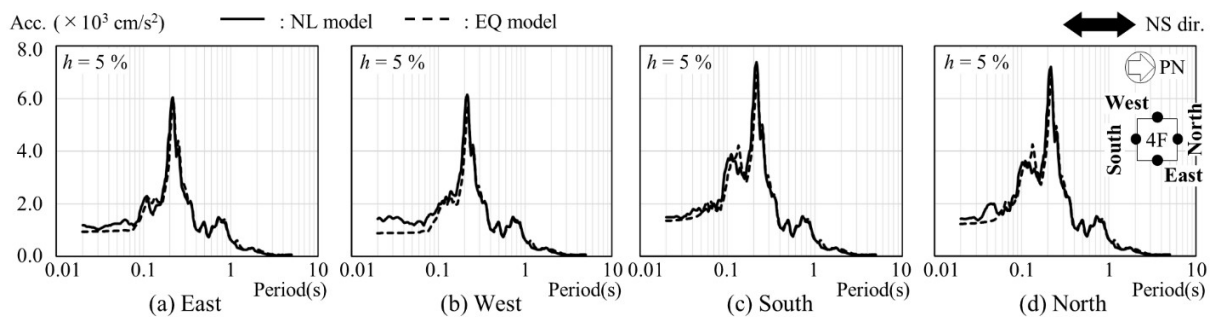


Fig. 15 Comparison of acceleration response spectra of four nodes at 4F (Ichihara et al., 2022b)

than that of the NL model in some areas, such as around the openings on 1F and 4F. The same trend is observed in Fig. 12, which demonstrates good agreement between Figs. 12 and 13.

Figure 14(A) presents the acceleration response contour in the out-of-plane direction of the external wall for each model. The figure indicates that the response values of both models tended to increase in the superstructure with the boundary at the GL, and the response was large in the upper part near the center of the 4F wall. The responses of the NL and EQ models were correlated well with each other, although there were local differences, which may be due to the effect of shear cracking in the wall of the superstructure with the boundary at the GL. Next, we focus on the difference in the maximum displacement response at each node. Figure 14(B) presents the displacement response contours for each model. The displacement responses in the figures were evaluated as relative displacements from the bottom edge of the base slab. Figure 14(B) shows that both models' displacement responses increased in the superstructure with the boundary at the GL, as in the acceleration contour. By comparing the NL and EQ models' responses, the overall difference within the wall was small, and the EQ model's responses were slightly larger.

Next, we compare the acceleration response spectra ( $h = 5\%$ ) of four nodes on 4F in the NS direction (Fig. 15). The response spectra of the four nodes on the floor at the east, west, north, and south sides all had a dominant period approximately 0.2 s, and the response spectra on the floor at the north and south sides had peaks approximately 0.1–0.15 s, which may be due to the out-of-plane response of the wall. Comparing the NL and EQ models, minor differences in the spectral shape, which may be due to shear cracking of the RC wall, were observed in the low-period region below 0.15 s, and the NL model's spectra slightly exceed those of the EQ model.

## CONCLUSION

This study's findings are as follows. During equivalent linear analysis using the EQ model, as the strain level increased, the plasticity of the structure increased in the superstructure with the boundary at the GL,

and the maximum shear strains in the walls of 1F, 4F, and CF, where the degree of plasticity was large, were approximately the same as or larger than those obtained in nonlinear analysis using the NL model. The out-of-plane maximum acceleration and displacement responses of the external wall obtained from the EQ model were generally consistent with the distribution of the NL model, although some of the acceleration at the top of the building, where the plasticity was increased locally, tended to be lower than that of the NL model. The acceleration response spectra on the floor of 4F at the east, west, north, and south sides correlated well with the NL model for the main peaks, such as the dominant frequency, width, and amplitude, although differences occurred in the shape of the low-period side between the NL and EQ models, which may be due to the effect of shear cracking.

In summary, this paper presents a basic study on the applicability of equivalent linear analysis proposed by Ghiocel (2015) to NPP facilities, focusing on the nonlinear response characteristics of RC seismic walls. However, this study involves limited conditions for equivalent linear analysis and limited seismic input and ideal soil conditions. To apply the results to actual buildings, such as RBs, it is necessary to accumulate sufficient knowledge through SSI analysis considering more complex soil effects and comparison with other test results, which will be addressed in future work.

## ACKNOWLEDGMENTS

This paper is based on the findings of the contract research entrusted from the secretariat of Nuclear Regulation Authority of Japan (NRA). In addition, Dr. Tsuyoshi Takada and Ph.D. Tadahiko Shiomi of the Japan Atomic Energy Agency (JAEA), and Dr. Tomohiro Horiguchi of Terrabyte Corporation provided invaluable advice in the preparation of this paper. We would like to express our gratitude to all of them.

## REFERENCES

- Cheng, Y. and Mertz, G. (1989). "Inelastic seismic response of reinforced concrete low-rise shear walls of building structures," *Univ. of Missouri-Rolla*, Dept. of Civil Eng, Civil Eng. Study Struct. Series 89-30, Univ. of Missouri-Rolla.
- Ichihara, Y. et al. (2021a). "Analysis of Influential Factors that Contribute to Precise Estimation of Three-Dimensional Seismic Building Behavior of Nuclear Facilities and Examinations of Applicability of its Setting Methods," NRA Technical Report Series No. NTEC-2021, 4002, NRA, Tokyo, Japan [in Japanese].
- Ichihara, Y. et al. (2021b). "3D FEM Soil-Structure Interaction Analysis for Kashiwazaki-Kariwa Nuclear Power Plant Considering Soil Separation and Sliding," Frontiers in Built Environment, Frontiers Media S.A., 7.
- Ichihara, Y. et al. (2022a). "Applicability of Equivalent Linear Analysis to Reinforced Concrete Shear Walls: 3D FEM Simulation of Experiment Results of Seismic Wall Ultimate Behavior," *Trans. At. Energy Soc. Japan, action of the Atomic*, 21, Japan [in Japanese].
- Ichihara, Y. et al. (2022b). "Basic Study on Seismic Response of Soil-Structure Interaction System Using Equivalent Linear Three-Dimensional FEM Analysis of Reactor Building," *J Struct. Eng. AJI*, 68B Japan. [in Japanese].
- IAEA (2013). "Review of Seismic Evaluation Methodologies for Nuclear Power Plants Based on a Benchmark Exercise," IAEA TECDOC, 1722, IAEA, Vienna.
- Japan Electric Association (JEA) (2017). "Technical Code for Seismic Design of Nuclear Power Plants JEAC-4601–2015," JEA, Japan. [in Japanese].
- Ghiocel, D. (2015). "Fast Nonlinear Seismic SSI Analysis Using a Hybrid Time-Complex Frequency Approach Frequency Approach for Low-Rise Nuclear Concrete Shearwall Buildings" in Proc. 23rd SMiRT conference, Manchester, UK.
- Ghiocel Predictive (GP) Technologies, Inc. (2019). "ACS SASSI Version 4.1 (IKTR1) Main Software User Manual Revision 2," GP Technologies Inc, New York, USA.
- Nakamura, N. et al. (2010). "Study of Ultimate Seismic Response and Fragility Evaluation of Nuclear Power Building Using Nonlinear Three-Dimensional Finite Element Model," *Nucl. Eng. Des.*, 240, 166-180.
- OECD/NEA/CSNI (1996). "Seismic Shear Wall ISP NUPEC's Seismic Ultimate Dynamic Response Test - Comparison Report," *NEA/CSNI/R* (96)10, OECD/GD (96)188.
- Schnabel, B., Lysmer, J. and Seed, H.B. (1972). "SHAKE-A Computer Program for Earthquake Response Analysis of Horizontally Layered Sites," Report No. EERC72-12, EERC, California, USA.